The Journal of Chemical Physics

Temporary anion states of fluorine substituted benzenes probed by charge transfer in $O_2^-{\cdot}C_6H_{6-x}F_x$ (x = 0–5) ion–molecule complexes

Cite as: J. Chem. Phys. **152**, 204309 (2020); https://doi.org/10.1063/5.0011321
Submitted: 20 April 2020 . Accepted: 08 May 2020 . Published Online: 28 May 2020

Marissa A. Dobulis, Michael C. Thompson, Thomas Sommerfeld, and Caroline Chick Jarrold

The Journal of Chemical Physics ARTICLE scitation.org/journal/jcp

Temporary anion states of fluorine substituted benzenes probed by charge transfer in $O_2^-{\cdot}C_6H_{6-x}F_x$ (x = 0–5) ion–molecule complexes

Cite as: J. Chem. Phys. 152, 204309 (2020); doi: 10.1063/5.0011321
Submitted: 20 April 2020 • Accepted: 8 May 2020 •
Published Online: 28 May 2020

Marissa A. Dobulis,[1] Michael C. Thompson,[1] Thomas Sommerfeld,[2] and Caroline Chick Jarrold[1,a)]

AFFILIATIONS

[1]Department of Chemistry, Indiana University, 800 East Kirkwood Avenue, Bloomington, Indiana 47405, USA
[2]Department of Chemistry and Physics, Southeast Louisiana University, SLU 10878, Hammond, Louisiana 70402, USA

[a)]**Author to whom correspondence should be addressed:** cjarrold@indiana.edu

ABSTRACT

The broadband photoelectron source realized by detaching $O_2^-{\cdot}X$ (X = neutral unsaturated molecule) complexes offers a unique opportunity to probe temporary anion states of the unsaturated species. Detachment of the ion molecule complex typically accesses a dissociative portion of the neutral potential, creating a continuum electron source that can undergo scattering with X. We present the application of this new approach to electron-neutral scattering toward a study of the series of fluorinated benzenes via photoelectron spectroscopy of $O_2^-{\cdot}C_6H_{6-x}F_x$ (x = 0–6) measured with several photon energies. We compare these spectra to the reference $O_2^-{\cdot}$hexane spectrum and observe evidence of temporary anion states of $C_6H_{6-x}F_x$ for species with x = 0–5 in the form of enhanced signal intensity at electron kinetic energies coinciding with the energies of the temporary anions. Furthermore, we observe autodetachment features in the x = 3, 5 spectra. Results of calculations on the isolated symmetric isomer of $C_6H_3F_3$ suggest that the molecule cannot support a weakly-bound non-valence state that could be associated with the observed autodetachment. However, $C_6HF_5^-$ is predicted to support a valence bound state, which, if produced by charge transfer from O_2^- with sufficient vibrational energy, may undergo autodetachment. Finally, the $[O_2{\cdot}C_6F_6]^-$ spectrum is unique insofar as the spectrum is substantially higher in binding energy and qualitatively different from the x = 0–5 spectra. This result suggests much stronger interactions and charge delocalization between O_2^- and C_6F_6.

I. INTRODUCTION

Temporary anion states are fleeting manifestations of excess electron occupation of normally unoccupied orbitals of neutral molecules that are unstable with respect to electron loss. These states are of interest because of their importance in electron-driven chemical processes including redox reactions, electron attachment, which has astrochemical relevance,[1–3] and dissociative attachment, relevant in radiation-induced DNA damage[4–6] and charge carrier formation in the ionosphere.[7,8] Because of the transient and delocalized nature of electron-neutral interactions, theoretical treatment is particularly challenging.[9–11]

Simple closed shell organic molecules generally have negative electron affinities (EAs). That is, their anions are higher in energy than the corresponding neutral and shed the electron on a sub-picosecond timescale. In the case of unsaturated hydrocarbons, the presence and energies of low-lying valence anion states involving π^* occupancy have been measured by electron transmission spectroscopy.[12,13] The electron transmission spectrum of benzene, for example, exhibits vibrationally resolved variations in electron transmission at electron kinetic energies (e^-KE) around 1.1 eV, which reflects the energy of the $^2E_{2u}$ temporary anion state relative to the neutral.[14] Electron transmission spectral measurements have been recorded for a variety of substituted organic

molecules, such as benzenoids,[14,15] benzoates,[16,17] isonitriles,[18] haloalkenes and halobenzenes,[19–21] isothiocyanates,[22] and a wide range of heterocycles.[23–25]

We recently observed evidence of charge transfer to benzene's $^2E_{2u}$ temporary anion state in the anion photoelectron (PE) spectrum of the O_2^-·benzene and O_4^-·benzene ion–molecule complexes (IMCs).[26] Striking enhancement of the electron signal at e^-KE values near 1 eV was observed over the broad and unresolved photoelectron signal characteristic of the PE spectra of these IMCs. Figure 1 shows the relative energies of the initial anion and neutral states of the $O_2^{(-)}$·benzene complex (solid lines), along with the approximate zero-point energies of the temporary O_2·benzene$^-$ states (dashed lines). For reference, the PE spectrum of bare O_2^- is shown in the top panel as the red trace, to illustrate the extended vibrational progressions for all three electronic transitions accessed by detaching the anion with 3.495 eV photon energy, along with the O_2^-·benzene PE spectrum (blue trace). Bands **X** and **a** in the spectrum of O_2^-·benzene correspond to the final neutral states in which O_2 is in the $X\ ^3\Sigma_g^-$ and $a\ ^1\Delta_g$ states, respectively.

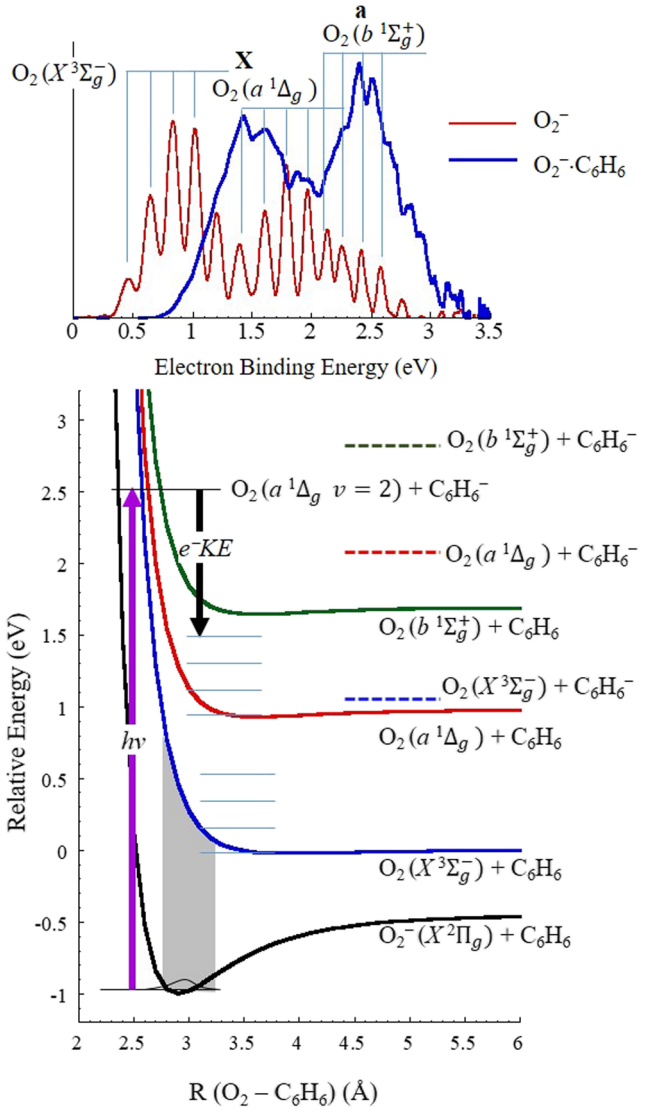

FIG. 1. Top: O_2^- (red trace) and $O_2^-\cdot C_6H_6$ (blue trace) 3.495 eV photoelectron spectra. The origins of the transitions to the $X^3\Sigma_g^-$, a $^1\Delta_g$, b$^1\Sigma_g^+$ O_2 states are marked with respect to the O_2^- spectrum. Bottom: potential energy curves along the $O_2^-(X^2\Pi_g)$·benzene and O_2·benzene dissociation coordinate. The dotted traces correspond to the O_2 ($X^3\Sigma_g^-$, blue; a $^1\Delta_g$, red; and b $^1\Sigma_g^+$, green) + $C_6H_6^-$ states, and the gray area corresponds to the Franck–Condon overlap between the initial anion and neutral ground states.

The neutral van der Waals complex formed by the photodetachment of the O_2^-·benzene IMC is on the repulsive part of the potential. Furthermore, the detachment spectrum of O_2^- has extended vibrational manifolds due to the significant difference in O_2^- and O_2 bond distances,[27] and consequently, fixed-frequency detachment of the IMC produces a broad continuum of e^-KE values. Importantly, because the portion of the neutral potential with Franck–Condon overlap with the initial IMC is repulsive, a single photon energy can be resonant with a range of O_2·benzene$^-$ charge transfer states. For example, the 3.495 eV photon energy used in the previous[26] and current studies is resonant with the O_2 ($a\ ^1\Delta_g v' = 2$) + benzene$^-$ state, in which the two molecular species are formed with modest repulsion, or the benzene$^-$ is formed with modest vibrational energy. The final O_2 ($a\ ^1\Delta_g$) + benzene state produces e^-KE values in the range of 0.5–1.5 eV, which encompasses the known $^2E_{2u}$ temporary anion state of benzene.[14]

The energy of the temporary valence anion states of substituted benzene is predicted to decrease with the substitution of electron-withdrawing groups, as reported by Driver and Jena, who calculated the electron affinities (EAs) of the $C_6H_{6-x}F_x$ (x = 0–6) series.[28] The EA was predicted to be negative for $C_6H_{6-x}F_x$ (x = 0–3), near-zero for tetrafluorobenzene (x = 4), and positive for pentafluorobenzene and hexafluorobenzene (x = 5, 6). Hexafluorobenzene is known to have a more strongly bound valence anion state in addition to a diffuse, non-valence-bound state (NVBS) lying ~100 meV below the detachment continuum.[29] Verlet and co-workers have studied the dynamics of low e^-KE electron attachment to the bound valence state through the NVBS.[30] This study leveraged the production of low-kinetic energy electrons by near-threshold detachment of I^- in an IMC with hexafluorobenzene, $I^-\cdot C_6F_6$, which essentially provided the pathway for gentle electron attachment to the C_6F_6 molecule to form the non-valence state. A similar strategy was used by Neumark and co-workers to affect charge transfer and to study the electron attachment and dissociation dynamics via excitation of I^-·uracil[31] and I^-·uracil·H_2O complexes.[32] Historically, IMCs have been used to explore charge-transfer intermediates in S_N2 reactions such as $I^-\cdot CH_3I$,[33] which inspired a number of related studies.[34–36] Of course, temporary anion states are also present in molecules that have valence bound states.[37]

Below, we report a study of low-energy temporary anion states of $C_6H_{6-x}F_x^-$ accessed by charge transfer initiated from $O_2^-\cdot C_6H_{6-x}F_x$ ($0 \le x \le 5$) IMC excitation and evidenced by a clear enhancement of portions of the broad spectral signal observed in the PE spectra. We additionally observe evidence of autodetachment from vibrationally excited non-valence bound states of the $[O_2\cdot C_6H_{6-x}F_x]^-$ (x = 3, 5) complexes.

II. METHODS

A. Experimental

The anion photoelectron imaging (PEI) apparatus has been described elsewhere;[38] therefore, a brief description follows. Mixtures of Ar, O_2, and room temperature fluorobenzenes (the highest molecular symmetry isomers of each were chosen for this study) were co-expanded using a pulsed molecular beam valve through a needle electrical discharge[39] stabilized by electrons generated from a hot, biased, thoriated iridium filament. The gas mixture passed through a skimmer, and the anions were accelerated to 1 keV. The ions were re-referenced to ground with a potential switch[40] prior to entering a Bakker-style time-of-flight mass spectrometer.[41,42] Anions of interest were selectively photodetached using the second (532 nm, 2.330 eV) and third (355 nm, 3.495 eV) harmonic outputs of a Nd:YAG laser (Continuum Surelite) or the output of a Nd:YAG pumped tunable optical parametric oscillator (Eskpla 240). Photoelectrons were extracted using a velocity map imaging lens system,[43] and the images were recorded on a dual microchannel plate-phosphor screen detector with a CCD camera.[44,45] Three-dimensional PE velocity distributions are obtained using BASEX[46] and then converted to electron kinetic energy (e^-KE). Photoelectron spectra are generally plotted as a function of electron binding energy, $e^-BE = h\nu - e^-KE$, as binding energies measured for typical direct detachment transitions are independent of photon energy. Calibrations based on the well-known PE spectrum of O_2^- were performed for each complex.[27] The pBASEX code was used for image reconstructions for the purpose of calculating the asymmetry parameter, β (E), because it avoids the centerline artifacts generated by BASEX.[47]

B. Theoretical

Because most of the spectra exhibited signatures of autodetachment from vibrationally excited non-valence bound states, calculations on the properties of the full series of substituted benzenes were completed to determine whether they would intrinsically support a NVBS, as was determined previously for C_6F_6.[29] Structures for all isomers of each $C_6H_{6-x}F_x$ (x = 1–5) molecule were optimized using MP2/ma-def2-TZVP(-f).[48,49] These geometries were used to determine polarizability, dipole moments, and quadrupole moments using MP2/def2-TZVPD.[47,50] Electron affinities calculated using the EA-EOM-CCSD/aug2 + 8s8p8d method, which directly computes the electron attachment energies of the molecule, are described in more detail elsewhere.[51] A more thorough search for NVBS in the $O_2{\cdot}C_6H_{6-x}F_x$ (x = 1–5) molecular complexes, with the charge associated more with the $C_6H_{6-x}F_x$ (x = 1–5) molecule, is complicated by coupling between the triplet ground state of O_2 and the doublet anion of the substituted benzene and will be presented in a subsequent report.

III. RESULTS AND ANALYSIS

A. Anion PE spectra

Figures 2(a)–2(g) show the PE spectra of the $O_2^-{\cdot}C_6H_{6-x}F_x$ ($0 \le x \le 6$) IMCs collected using the 3.495 eV photon energy (black trace). As noted above, the highest symmetry isomers of $C_6H_{6-x}F_x$ molecules that have multiple isomers were chosen. In other words, for x = 2–4, 1,4-difluorobenzene, 1,3,5-trifluorobenzene, and 1,2,4,5-tetrafluorobenzene, respectively, all of which have zero dipole moments due to their symmetries, were used in this study.

In order to determine which spectral features are affected by resonance with temporary anion states, we compare them directly to a similar system that exhibits the same spectral broadening, but is not affected by low-lying temporary anion states. In this case, we use the PE spectrum of the $O_2^-{\cdot}$hexane IMC,[26] shifted modestly to higher binding energy to match the transition energies of the $O_2^-{\cdot}C_6H_{6-x}F_x$ ($0 \le x \le 5$) spectrum. It is shown superimposed as the dotted trace in panels (a)–(f). As the binding energy increases with increasing fluorination in each $O_2^-{\cdot}C_6H_{6-x}F_x$ ($0 \le x \le 5$) spectrum, this shift is not constant, but varies between 0.10 eV for $O_2^-{\cdot}C_6H_6$ to 0.8 eV for $O_2^-{\cdot}C_6HF_5$. Hexane, a saturated hydrocarbon, stabilizes O_2^- by a comparable energy to benzene,[26] but the LUMU energy is much higher than that of unsaturated species. Furthermore, transitions to the O_2 ($X\ ^3\Sigma_g^-$)·hexane and O_2 ($a\ ^1\Delta_g$)·hexane states have the same relative intensities as the analogous transitions in bare O_2, but are broadened by the Franck–Condon overlap with the dissociative portion of the O_2^- hexane intermolecular potential in a way that is similar to the detachment transitions observed for O_2^-·benzene. Band X in both the O_2^-·hexane and O_2^-·benzene IMCs exhibits shoulders associated with the O_2 stretch progression, which allows close alignment of the spectra on the e^-BE scale. We, therefore, use this spectrum as a control for identifying anomalous intensities in the spectra of the $O_2^-{\cdot}C_6H_{6-x}F_x$ series of IMCs. For further confirmation, the spectrum of O_2^-·cyclohexane was also recorded and compared to the $O_2^-{\cdot}C_6H_{6-x}F_x$ spectra (included in the supplementary material), to show that the enhancements observed are independent of the control, assuming that the control (in this case, hexane or cyclohexane) does not present resonances.

The red trace in each spectrum is the difference between the $O_2^-{\cdot}C_6H_{6-x}F_x$ ($0 \le x \le 5$) IMCs and shifted O_2^-·hexane traces (difference spectra generated using O_2^-·cyclohexane are included in the supplementary material). Because each spectrum could exhibit resonances in different energy regions in the PE spectra, some coinciding with direct detachment band intensity maxima, the O_2^-·hexane spectrum was scaled for each $O_2^-{\cdot}C_6H_{6-x}F_x$ spectrum to minimize any negative difference signal. This approach is based on the assumption that resonances would only enhance the signal rather than deplete the signal.

Band **X** in the spectrum of $O_2^-{\cdot}C_6F_6$ [Fig. 2(g)] is significantly narrower than the lowest energy transitions in the PE spectra of either O_2^- or $C_6F_6^-$[52–54] and is at a substantially higher binding energy. As such, it appears to deviate from a system that can be described as an IMC in which the charge carrier is O_2, and we do not attempt to evaluate the spectral intensity anomalies using the PE spectrum of O_2^-·hexane as a control in this case. EAs and vertical detachment energies (VDEs), which are the energies at which the electronic transition reaches maximum intensity, determined from band **X** in each case [the O_2 ($X\ ^3\Sigma_g^-$)·$C_6H_{6-x}F_x$ final neutral state] are summarized in Table I.

Overall, the EA of the complexes increases with x. This observation suggests that increasing electron withdrawing substituents on the benzene ring results in stronger interactions between the O_2^- and $C_6H_{6-x}F_x$, while the intermolecular attraction in the *neutral* van der Waals attraction remains relatively small compared to the

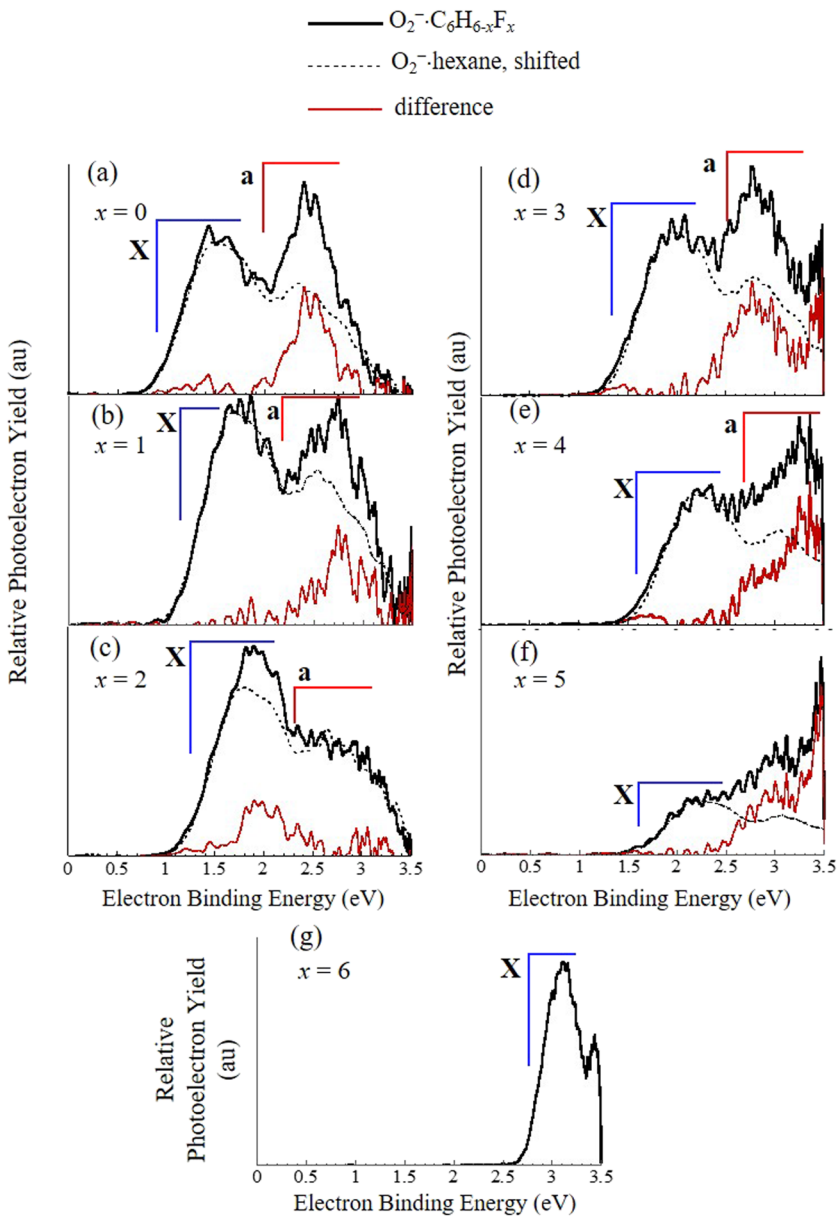

FIG. 2. 3.495 eV PE spectra of O_2^-·$C_6H_{6-x}F_x$ ($0 \le x \le 6$) (black trace) plotted in terms of electron binding energy. For $0 \le x \le 5$, the O_2^-·hexane spectrum is overlaid as the dotted black trace, shifted and scaled, so that the **X** (x = 0, 1, 3, 4) or **a** (x = 2) bands overlap. The red trace is the difference between the O_2^-·$C_6H_{6-x}F_x$ and O_2^-·hexane spectra.

increased attraction between O_2^- and $C_6H_{6-x}F_x$. In other words, the attractive potential for O_2^- + C_6H_6 shown as the solid black trace in Fig. 1 deepens with x, while the neutral curves remain relatively unchanged. This results in an increase in electron binding energy. The increasing O_2^-–$C_6H_{6-x}F_x$ interaction with x echoes the increasing electron binding energy calculated for bare $C_6H_{6-x}F_x$ with x, due to increasing depletion of charge in the σ-bonds in the C_6 ring, stabilizing the π and π* orbitals.[28] While a more detailed description of the molecular structures of these complexes will be included in a subsequent report, there is no clear correlation between the IMC structures with the O_2^- situated in the plane of the $C_6H_{6-x}F_x$ (with the O_2^- molecular axis either parallel to the plane or twisted out of the plane), strongly favored for x = 0–2, 4, or structures in which the O_2^- is above a C–F bond, favored for x = 5, 6. These two motifs are nearly isoenergetic for O_2^-·$C_6H_3F_3$.

B. Difference spectra

There is a clear x-dependent change in energy at which enhancement of the electron signal is observed in the spectra of O_2^-·$C_6H_{6-x}F_x$ ($0 \le x \le 5$). Figure 3 shows the difference spectra plotted vs e^-KE, which are directly comparable to electron transmission spectra. The red arrows on each spectrum indicate the EA calculated by Driver and Jena,[28] and the blue arrows are the

TABLE I. A summary of approximate adiabatic electron affinities of $O_2 \cdot C_6H_{6-x}F_x$ and the positions and the vertical energies and bandwidths of the temporary anion states.

	EA (eV)	VDE (eV)	ADE of temporary anion state relative (e^-KE, eV)	VDE of temporary anion state (e^-KE, eV)	Energy of anion to neutral: Calc.[a] (ETS)[b]
$O_2 \cdot C_6H_6$	0.90	1.52	0.8(2)	1.0	1.15 (1.09)
$O_2 \cdot C_6H_5F$	1.11	1.72	0.5(2)	0.72	0.93 (0.87, 1.48)
$O_2 \cdot C_6H_4F_2$	1.23	1.86	0.3, 1.2	0.42, 1.52	0.62/(0.65,1.38)
$O_2 \cdot C_6H_3F_3$	1.36	1.98	[c], 0.4	[c], 0.72	0.42
$O_2 \cdot C_6H_2F_4$	1.60	2.22	0.05, 0.5	0.19, 0.71	−0.01
$O_2 \cdot C_6HF_5$	1.61	2.24	[c], 0.25	[c], 0.53	−0.45
$O_2 \cdot C_6F_6$	2.75	3.11	...	...	−0.75

[a]Reference 28.
[b]References 19–20.
[c]The associated anion lies below the detachment continuum as indicated by the asterisks (*) in Fig. 7.

energies of temporary anion states measured by electron transmission for $x = 0$–2.[19,20]

There is not a simple monotonic shift in the energies of the difference spectra. We point out the degenerate $^2E_{2u}$ temporary anion state of benzene splits into two close-lying states in species with symmetry lower than D_{3h} (i.e., only 1,3,5-trifluorobenzene would have a degenerate temporary anion state). Electron kinetic energies at which the difference signal emerges, both the lower limit, which would reflect an adiabatic attachment energy, and e^-KE at which the signal reaches maximum intensity (vertical attachment energy) are included in Table I.

We first consider (a) $O_2^- \cdot C_6H_6$, (b) $O_2^- \cdot C_6H_5F$, and (c) $O_2^- \cdot C_6H_4F_2$, which exhibit resonances at decreasing e^-KE values that track the calculated EA[28] and electron transmission data.[19,20] The difference spectrum of $O_2^- \cdot C_6H_4F_2$ [Fig. 3(c)] exhibits a pronounced *excited* temporary anion state in addition to lower intensity enhancement associated with the ground temporary anion state, while in the case of the $O_2^- \cdot C_6H_5F$ [Fig. 3(b)], the relative intensities are opposite. This observation is consistent with how pronounced these states appear in the electron transmission spectra.[19,20]

The difference spectrum of $O_2^- \cdot C_6H_3F_3$ [Fig. 3(d)] exhibits a sharp and intense signal near threshold in addition to a broad resonance centered at 0.72 eV, which is higher in energy than that predicted by Jena[28] (there are no electron transmission data available for any isomer of trifluorobenzene). This may simply be the result of the state having a much broader vibrational manifold. Indeed, with increasing fluorination and decreasing temporary anion state energy, more pronounced structural differences between the temporary anion and neutral would result from tighter temporary binding of an electron in the antibonding orbital, resulting in a broader vibrational manifold. The single resonance is consistent with the D_{3h} symmetry of this molecule; while the degeneracy of the temporary anion state in benzene is broken in fluorobenzene and 1,4-difluorobenzene, the temporary anion state is degenerate in 1,3,5-trifluorobenzene. Moreover, the broad resonance has a partially resolved, extended 1120 ± 20 cm^{-1} progression, indicated by the green comb in Fig. 3(d), which is close to 1128–1129 cm^{-1} measured for the ν_{11} vibrational mode of the neutral.[55] This mode has e′ symmetry and involves the degenerate, in-plane distortion of the ring. As such, it is consistent with promoting an electron into the degenerate π^* LUMO of 1,3,5-trifluorobenzene. However, the appearance of a signal with nearly zero kinetic energy is indicative of autodetachment from excited vibrational (or rotational) levels of a weakly *bound* anion. This effect will be explored more below.

The spectra of the more fluorinated species, $x = 4$, 5, have profiles that depart more substantially from the O_2^- spectral profile. However, band **X** in both spectra follows the same contour as band **X** in the O_2^-·hexane control spectrum, and the difference signal observed is consistent with calculated EAs.[28] The difference spectrum of $O_2^- \cdot C_6H_2F_4$ [Fig. 3(e)] exhibits a broad signal increasing from e^-KE ~0 reaching a maximum at 0.19 eV, with an additional broad shoulder of signal between 0.5 eV and 1.0 eV, which is indicative of an excited temporary anion state. As will be further supported below, our result suggests that the EA of 1,2,4,5-tetrafluorobenzene is slightly negative, while Drive and Jena predict the EA of 1,2,3,5-tetrafluorobenzene to be +0.01 eV.[28]

The $O_2^- \cdot C_6HF_5$ difference spectrum [Fig. 3(f)], as with the $O_2^- \cdot C_6H_3F_3$ difference spectrum [Fig. 3(d)], exhibits an intense signal near threshold, which could be due to autodetachment from vibrationally excited levels of the bound state of $C_6HF_5^-$. Driver and Jena predicted a 0.45 eV electron binding energy.[28] Again, with C_{2v} symmetry, the orbitals correlated with the degenerate e_{2u} orbitals in benzene are split, and we assign the broad shoulder of signal peaking at approximately 0.5 eV as an excited and temporary anion state of this molecule.

C. Verifying temporary and weakly bound anion states

As noted above, the direct detachment signal collected using different photon energies appear at constant e^-BE value. In contrast, the signal enhanced due to resonance with a temporary anion state generally would appear at common e^-KE values when generated with different photon energies, as long as electrons within the range of the resonant e^-KE values are being produced. Therefore, spectra measured with different photon energies plotted against e^-BE will have differences in the spectroscopic features if temporary anion states are affecting the signal intensity. In addition, the signal appearing near threshold that is inconsistent with direct

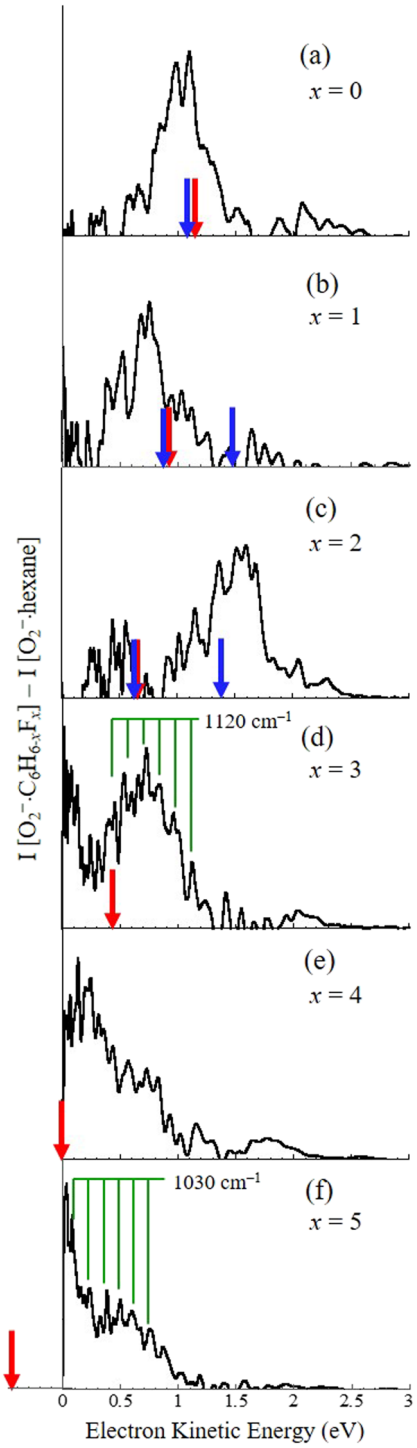

FIG. 3. $O_2^-\cdot C_6H_{x-6}F_x$–$O_2^-\cdot$hexane difference spectra for $0 \le x \le 5$. The red arrows on each spectrum indicate the EA calculated by Driver and Jena (Ref. 28), and the blue arrows are the energies of temporary anion states measured by electron transmission (Refs. 19 and 20). Green combs indicate vibrational spacings noted in the text. We note that the $x = 4$ calculated EA from Ref. 28 results from 1,2,3,5-tetrafluorobenzene instead of 1,2,4,5-tetrafluorobenzene.

detachment features measured over different wavelengths is often due to autodetachment of electrons from weakly bound valence states or non-valence bound states of anions, for which modest rovibrational excitation places the energy of the anion above the detachment limit. We, therefore, measured the spectra of the $O_2^-\cdot C_6H_{6-x}F_x$ ($0 \le x \le 5$) complexes using the 2.330 eV photon energy and, when further clarification was necessary, the 2.870 eV photon energy.

Figures 4(a)–4(f) and 5(a)–5(f) show spectra measured with 3.495 eV (purple traces), 2.330 eV (green traces), and in several cases, 2.870 eV (blue traces) photon energies, plotted against e^-BE and e^-KE, respectively. Band **X** in the PE spectrum of $O_2^-\cdot C_6H_6$ [Fig. 4(a)] is subtly narrower in the 2.330 eV spectrum than in the 3.495 eV spectrum, consistent with resonance enhancement over a narrower energy range than the unperturbed width of band **X**. This effect is more pronounced with the comparison of the 2.330 eV and 3.495 eV spectra of $O_2^-\cdot C_6H_5F$ [Fig. 4(b)]. We additionally obtained the 2.870 eV spectrum of $O_2^-\cdot C_6H_5F$ to determine whether the low-intensity threshold signal in the 3.495 eV spectrum was due to autodetachment; absence of threshold signal in the lower photon energy spectra suggests that it is not. Band **X** in the 2.870 eV spectrum is clearly broadened by the resonance centered at e^-KE = 0.72 eV. Referring to Figs. 5(a) and 5(b), it is evident that the profile of band **X** in both cases has overlap with the $C_6H_6^-$ and $C_6H_5F^-$ temporary anion states (black traces), respectively. Indeed, the narrow profile of band **X** in the 2.330 eV spectrum of $O_2^-\cdot C_6H_5F$ is nearly identical to the difference spectrum, as can be seen in Fig. 5(b). The 2.330 eV and difference spectra are further directly compared in the supplementary material.

The PE spectrum of $O_2^-\cdot C_6H_4F_2$ was also measured at all three wavelengths. Band **X** in the 2.330 eV and 3.495 eV spectra had small but reproducible profile differences apparent in Fig. 4(c). However, band **X** in the 2.330 eV and 2.870 eV spectra are identical and appear at a slightly lower e^-BE value than band **X** in the 3.495 eV spectrum, supporting the appearance of the resonance at e^-KE values coinciding with the high e^-BE portion of band **X** in the 3.495 eV spectrum, as is evident from Fig. 5(c).

The PE spectrum of $O_2^-\cdot C_6H_3F_3$ in Fig. 4(d) exhibits an intense, near-threshold electron signal in spectra measured with all three photon energies, in addition to the broad resonance centered at e^-KE = 0.72 eV [Fig. 5(d)]. The threshold signal is again characteristic of a weakly-bound anion with sufficient vibrational energy to lie above the detachment continuum. Our calculations suggest that 1,3,5-trifluorobenzene does not have the properties to support a NVBS. These properties, and those of other $C_6H_{6-x}F_x$ molecules, are summarized in the supplementary material. 1,3,5-Trifluorobenzene, by symmetry, has no dipole moment, and the quadrupole moments and polarizability are below values that would support a correlation bound state. It is also not due to O_2^- autodetachment, which occurs for vibrational levels above v = 3 and exhibits the characteristic O_2^- vibrational spacing.[38] The lowest lying valence anion state of 1,3,5-trifluorobenzene is calculated to lie 0.42 eV above the neutral,[28] so this threshold signal may be due to a NVBS that exists because of the proximity of O_2,[56] a possibility that will be explored further in a subsequent report. We can eliminate the possibility that this signal arises from a two-photon process that results in F^- formation and subsequent F^- detachment, since both 2.330 eV and 2.870 eV photon energies are below the threshold for F^- detachment.

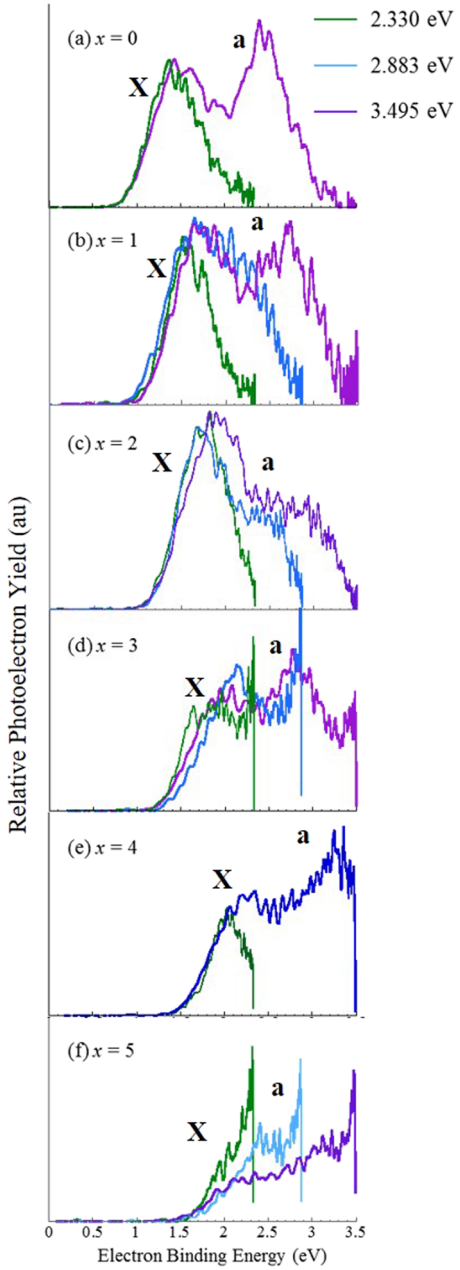

FIG. 4. Comparison of PE spectra of $O_2^- \cdot C_6H_{x-6}F_x$ ($0 \le x \le 5$) measured with 3.495 eV (purple traces), 2.330 eV (green traces), and in several cases, 2.870 eV (blue traces), plotted against $e^- BE$.

In contrast to the 1,3,5-trifluorobenzene analog, the spectra of $O_2^- \cdot C_6H_2F_4$ [Fig. 4(e)] exhibit no sharp signal at the threshold limit, and as such, no 2.870 eV spectrum was recorded. The spectra do show a fairly intense and broad enhancement reaching a maximum intensity at 0.19 eV, which, in the 2.330 eV spectrum, results in an enhancement in portions of band **X**. Both the 3.495 eV and

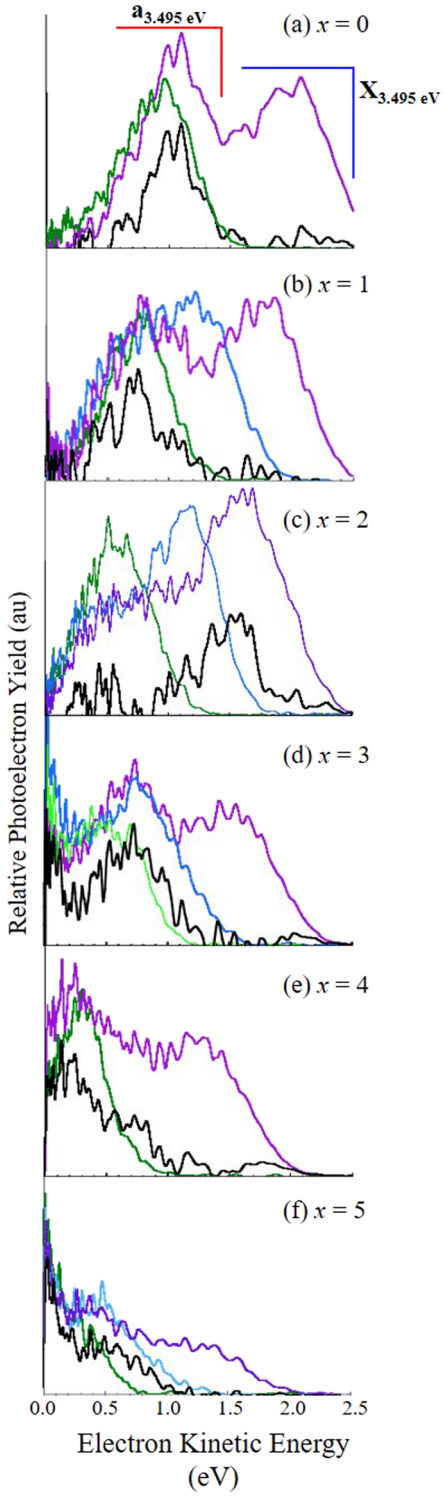

FIG. 5. Comparison of PE spectra of $O_2^- \cdot C_6H_{x-6}F_x$ ($0 \le x \le 5$) measured with 3.495 eV (purple traces), 2.330 eV (green traces), and in several cases, 2.870 eV (blue traces), along with the difference spectra (black traces), plotted against $e^- KE$.

2.330 eV O_2^-·$C_6H_2F_4$ spectra shown in Fig. 5(e) exhibit signal intensity that decreases as e^-KE decreases from 0.2 eV to 0 eV. This is consistent with a near-zero but marginally negative electron affinity. If the EA were positive, there would be an enhancement of the signal near threshold due to the $\Delta v = -1$ autodetachment propensity rule.

Spectra of O_2^-·C_6HF_5 shown in Fig. 4(f) measured with the three photon energies again exhibit a sharp and intense threshold signal. C_6HF_5 is predicted to bind an electron by 0.45 eV,[28] which is comparable to the binding energy of O_2 (0.448 eV).[27] Charge transfer from O_2^- to $C_6HF_5^{(-)}$ may excite a broad distribution of vibrationally excited levels of $C_6HF_5^-$, leading to autodetachment from the levels more than 0.45 eV above the zero point level. Interestingly, while the autodetachment signal has a low signal to noise ratio, there is a discernable recurrence of peaks spaced by 1030 ± 20 cm^{-1} [Fig. 3(f)], which may be due to high vibrational levels of the ν_6 (a_1 symmetry) mode, which has a harmonic frequency of 1079 cm^{-1} in the neutral.[57,58]

Calculations on the properties of C_6HF_5 (supplementary material) suggest that this molecule cannot support a NVBS, as was the case with all of the (highest symmetry) fluorine-substituted benzenes with $x < 6$. C_6HF_5 has a dipole moment of only 1.37 D below the critical dipole moment to access a dipole bound state.[59,60] Furthermore, the quadrupole moment is small. Based on past studies, this is interpreted as a 1 meV upper limit on electron binding energy. Our results suggest that ONLY C_6F_6 supports a NVBS, with a fairly robust binding energy of approximately 100 meV, in agreement with experiments.[30,53] However, further calculations on the O_2·C_6HF_5 IMC will be required before we can definitively assign the autodetachment signal to vibrationally excited levels of the valence anion state of C_6HF_5.

As a final point of comparison between the spectra, the photoelectron angular distributions (PADs) throughout the broad signal in the spectra also show striking differences among the different IMCs. Figure 6 includes a plot of the e^-KE-dependent asymmetry parameter [$\beta(E)$] determined from the following formula:

$$\beta(E) = \frac{I_0 - I_{90}}{\frac{1}{2}I_0 + I_{90}},$$

where I_0 and I_{90} are the relative intensities of electron signal parallel and perpendicular to the electric field of the detachment laser in terms of electron kinetic energy, for O_2^-·benzene (black) and O_2^-·hexane (red). The difference spectrum is plotted to compare the location of the resonances. These values result from the experimentally reconstructed images from the pBASEX code.[47] The plots for O_2^-·$C_6H_{6-x}F_x$ ($1 \le x \le 6$) are available in the supplementary material. For the IMCs, only the PADs resulting from the 3.495 eV photon energy detachment were considered. For detachment of bare O_2^-, the asymmetry parameter is negative but approaches 0 with decreasing e^-KE.[61] The same is true of the PAD in the spectrum of O_2^-·hexane. Since the spectra shift to lower e^-KE with increasing x, a direct comparison of the PADs is not straightforward. However, the PADs in the spectra of O_2^-·$C_6H_{6-x}F_x$ ($0 \le x \le 3$) complexes show the same general trend of increasing β with decreasing e^-KE, but with deviations from the O_2^-·hexane plot at energies coinciding with the resonances. The PADs determined for the spectra of O_2^-·$C_6H_{6-x}F_x$ ($4 \le x \le 6$) are positive, and correlation between the resonances and the PADs is not obvious, but this may simply be a reflection of the stronger interactions between O_2^- and $C_6H_{6-x}F_x$ ($4 \le x \le 6$) and more profound effect on the O_2-local π_g HOMO of the IMCs.

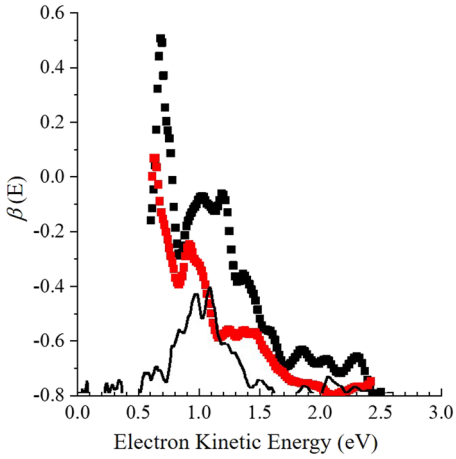

FIG. 6. O_2^-·hexane (red dotted trace) and O_2^-·C_6H_6 (black dotted trace) asymmetry parameters, calculated from the 3.495 eV photoelectron spectra, plotted in terms of electron kinetic energy. The difference spectrum O_2^-·C_6H_6 is overlaid in the black solid trace plotted in terms of electron kinetic energy for reference.

IV. DISCUSSION

To set the stage for discussion, Fig. 6 shows the approximate energies of the O_2^-·$C_6H_{6-x}F_x$ ($0 \le x \le 5$) IMCs relative to the free O_2 + $C_6H_{6-x}F_x$ ($0 \le x \le 5$) + e^- limit, along with the lowest e^-KE at which enhancement is observed, which we attribute to the formation of O_2·$C_6H_{6-x}F_x^-$ ($0 \le x \le 5$). Energies for both resonances are included in the case where more than one is observed. Bound states undergoing autodetachment from excited vibrational levels are indicated by an asterisk (*), since they lie below the O_2 + $C_6H_{6-x}F_x$ ($0 \le x \le 5$) + e^- limit by an energy that cannot be measured with the current experimental setup. For reference, the calculated energies[28] of the anions of free $C_6H_{6-x}F_x^-$ ($0 \le x \le 5$)[28] relative to O_2 + $C_6H_{6-x}F_x$ ($0 \le x \le 5$) + e^- limit are included, along with the energies of the temporary anion states measured using electron transmission methods for $0 \le x \le 2$.[19] We again note that the $x = 2$, 4 energies calculated by Driver and Jena[28] result from species with lower symmetry than those experimentally measured here.

Figure 7 shows the close agreement between Driver and Jena's calculated energies and those measured by electron transmission spectroscopy, while the energies determined from the current method lie systematically 0.3–0.4 eV below for $x = 0$, 1, and 2. This difference raises the question of whether the nearby O_2 molecule solvates the temporary anion states, lowering the energy of the temporary IMC relative to the free temporary anion. However, previous studies[38] on O_3^-·$[O_2]_n$ suggest that O_2 solvent molecules stabilize by ~0.1 eV in the case of a more localized charge, which is much lower than the difference between the energies shown in Fig. 6. A second possible source of the disparity is any distortion of the $C_6H_{6-x}F_x$

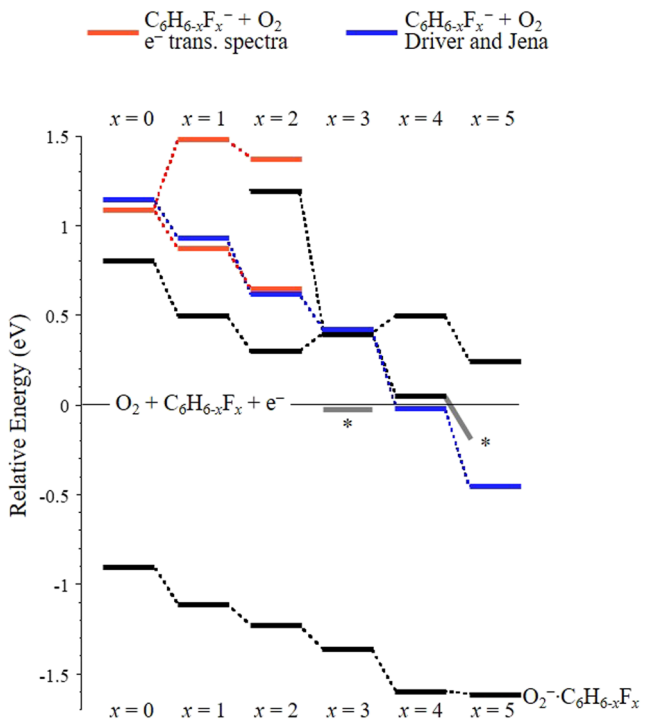

FIG. 7. Relative energies of temporary anion states of the $O_2 \cdot C_6H_{6-x}F_x$ (x = 0–5) as measured in this study (black), calculated by Driver and Jena (Ref. 28, blue), and measured in electron transmission studies (red, Refs. 19 and 20). The asterisks (*) correspond to states with autodetachment from vibrationally excited levels that cannot be measured by this experiment.

from the relaxed neutral structure, which would decrease the energy between the neutral (distorted) structure and the temporary anion. This effect is currently being explored further computationally, and the results will be presented in a subsequent report. Finally, electron transmission spectra,[19,20] which are typically presented as the derivative of transmitted current as a function of electron energy, indeed show sharp decreases in the differential current at the energies coinciding with the onset of enhancement in the spectra presented here. More thorough calculations on the IMCs may shed further light on the discrepancy between energies of the resonances in these spectra and the electron transmission data.

Figure 7 also clearly shows how the increasing stability of $C_6H_{6-x}F_x^-$ ($0 \le x \le 5$) tracks with the increasing electron binding energy of $O_2 \cdot C_6H_{6-x}F_x$ ($0 \le x \le 5$). This is readily rationalized by the increasing electrophilicity of the benzene ring with increasing x. However, C_6HF_5 is predicted to have an electron affinity comparable to O_2, raising the question of whether this complex can be described as a simple IMC, with charge localized on the O_2^-. The gradual increase in electron binding energy with x, up to $x = 5$, suggests that $O_2^- \cdot C_6HF_5$, in which a small anion is stabilized by a fairly polarizable molecule with a non-zero dipole (supplementary material), is an appropriate description of this IMC. However, this increase dramatically changes at $x = 6$, suggesting that this description would be inappropriate for $O_2^- \cdot C_6F_6$.

According to the computational results, as noted above, C_6F_6 is the only F-substituted benzene in the highest symmetry $C_6H_{6-x}F_x^-$ ($0 \le x \le 6$) series to support a NVBS. This result is puzzling because while $C_6H_{6-x}F_x^-$ ($0 \le x \le 5$) could, in principle, have ~1 meV binding energies, why would C_6F_6 have the relatively robust binding energy of 100 meV? It surely is not its polarizability; the differences are not that large between $x = 6$ and $0 \le x \le 5$. Additionally, the quadrupole moment of C_6F_6 is not exceptionally large (Q_{xx} = 6.06 atomic units). It is possible that the alignment of the quadrupole with the nuclear framework may be involved, but again, the factor of one hundred increase in electron binding energy cannot be explained by something so subtle.

The $[O_2 \cdot C_6F_6]^-$ spectrum is qualitatively different from the other $O_2^- \cdot C_6H_{6-x}F_x$ spectra. Band **X** is substantially narrower and at a significantly higher binding energy (VDE = 3.10 ± 0.05 eV). This blue shift is also greater than those previously observed in $[X \cdot C_6F_6]^-$ clusters.[62] This result raises interesting questions about whether the relatively strongly bound NVBS of $C_6F_6^-$ is somehow involved in supporting a much stronger molecular complex anion, a question that will be addressed in a subsequent report.

V. CONCLUSIONS

The PE spectra of $O_2^- \cdot C_6H_{6-x}F_x$ IMCs ($0 \le x \le 6$) are reported; all exhibit spectroscopic features that deviate from those of a simple O_2^-·alkane PE spectrum. The spectra of species with $0 \le x \le 5$ exhibit a broad, unresolved detachment signal that appears at higher e^-BE values with increasing F-substitution. However, the broadband photoelectron signal generated by detachment of $O_2^- \cdot C_6H_{6-x}F_x$ is enhanced at x-dependent e^-KE due to resonances with temporary anion states of the unsaturated species. In this regard, the photoelectrons are a tool for probing temporary anion states of the neutral partner in the IMC.

Detachment of these IMCs typically accesses a dissociative portion of the neutral potential due to stronger interactions in an IMC vs the associated neutral van der Waals complex, which results in the continuum electron source. We compare the spectra of $O_2^- \cdot C_6H_{6-x}F_x$ IMCs ($0 \le x \le 5$) to the reference O_2^-·hexane spectrum and observe evidence of temporary anion states of $C_6H_{6-x}F_x$ for species with $0 \le x \le 5$ in the form of enhanced signal intensity at electron kinetic energies coinciding with the energies of the temporary anions.

Furthermore, autodetachment features are observed at the low-e^-KE limit in the x = 3, 5 spectra. Based on theoretical considerations, the symmetric $C_6H_3F_3$ molecule used in this study does not have the physical properties that would support a non-valence bound anion state, suggesting that the bystander O_2 helps support a non-valence bound state in the complex. $C_6HF_5^-$, on the other hand, is predicted to support a valence bound state, which,[28] if produced by charge transfer from O_2^- with sufficient vibrational energy, may undergo autodetachment. Finally, the $[O_2 \cdot C_6F_6]^-$ spectrum is unique insofar as the spectrum is substantially higher in binding energy and qualitatively different from the $0 \le x \le 5$ spectra. This result suggests much stronger interactions and charge delocalization between O_2^- and C_6F_6. A more thorough theoretical exploration of the subtle interactions between O_2^- and $C_6H_{6-x}F_x$ will be presented in a subsequent report.

SUPPLEMENTARY MATERIAL

The supplementary material includes additional experimental results, including raw and reconstructed images, the O_2^-·cyclohexane 3.495 eV PE spectrum, O_2^-·cyclohexane difference spectra, and plots of asymmetry parameters of 3.495 eV photon energy spectra, and the theoretical results on the physical properties of the isolated F-substituted benzene molecules, which suggest none can support a non-valence-bound anion state.

ACKNOWLEDGMENTS

C.C.J. gratefully acknowledges support for this research from the National Science Foundation, Grant No. CHE-1664965. T.S. gratefully acknowledges support from the National Science Foundation under Grant No. 1856775.

DATA AVAILABILITY

The data that support the findings of this study are available from the corresponding author upon reasonable request.

REFERENCES

[1] P. J. Sarre, Mon. Not. R. Astron. Soc. **313**, L14 (2000).
[2] N. J. Mason, B. Nair, S. Jheeta, and E. Szymańska, Faraday Discuss. **168**, 235 (2000).
[3] K. Graupner, T. A. Field, and G. C. Saunders, Astrophys. J. **685**, L95 (2008).
[4] J. Simons, Acc. Chem. Res. **39**, 772 (2006).
[5] B. Boudaïffa, P. Cloutier, D. Hunting, M. A. Huels, and L. Sanche, Science **287**, 1658 (2000).
[6] H.-Y. Chen, P.-Y. Yang, H.-F. Chen, C.-L. Kao, and L.-W. Liao, J. Phys. Chem. B **118**, 11137 (2014).
[7] G. Senn, J. D. Skalny, A. Stamatovic, N. J. Mason, P. Scheier, and T. D. Märk, Phys. Rev. Lett. **82**, 5028 (1999).
[8] J. Kitayama and M. Kuzumoto, J. Phys. D: Appl. Phys. **32**, 3032 (1999).
[9] A. F. White, M. Head-Gordon, and C. W. McCurdy, J. Chem. Phys. **146**, 044112 (2017).
[10] A. F. White, C. W. McCurdy, and M. Head-Gordon, J. Chem. Phys. **143**, 074013 (2015).
[11] M. F. Falcetta, L. A. DiFalco, D. S. Ackerman, J. C. Barlow, and K. D. Jordan, J. Phys. Chem. A **118**, 7489 (2014).
[12] K. D. Jordan, J. A. Michejda, and P. D. Burrow, Chem. Phys. Lett. **42**, 227 (1976).
[13] K. D. Jordan and P. D. Burrow, Acc. Chem. Res. **11**, 341 (1978).
[14] P. D. Burrow, J. A. Michejda, and K. D. Jordan, J. Chem. Phys. **86**, 9 (1987).
[15] M. Venuti and A. Modelli, J. Chem. Phys. **113**, 2159 (2000).
[16] S. A. Pshenichnyuk and A. Modelli, J. Chem. Phys. **136**, 234307 (2012).
[17] A. Modelli and S. A. Pshenichnyuk, J. Phys. Chem. A **116**, 3585 (2012).
[18] I. P. Csonka, L. Szepes, and A. Modelli, J. Mass Spectrom. **39**, 1456 (2004).
[19] J. K. Olthoff, J. A. Tossell, and J. H. Moore, J. Chem. Phys. **83**, 5627 (1985).
[20] J. C. Giordan, J. H. Moore, and J. A. Tossell, J. Am. Chem. Soc. **106**, 7397 (1984).
[21] Y. Choi and K. D. Jordan, Chem. Phys. Lett. **156**, 450 (1989).
[22] A. Modelli and D. Jones, J. Phys. Chem. A **110**, 13195 (2006).
[23] A. Modelli, B. Hajgató, J. F. Nixon, and L. Nyulászi, J. Phys. Chem. A **108**, 7440 (2004).
[24] A. Modelli, P. Bolognesi, and L. Avaldi, J. Phys. Chem. A **115**, 10775 (2011).
[25] A. Modelli and S. A. Pshenichnyuk, Phys. Chem. Chem. Phys. **15**, 1588 (2012).
[26] K. M. Patros, J. E. Mann, and C. C. Jarrold, J. Phys. Chem. A **120**, 7828 (2016).
[27] K. M. Ervin, I. Anusiewicz, P. Skurski, J. Simons, and W. C. Lineberger, J. Phys. Chem. A **107**, 8521 (2003).
[28] N. Driver and P. Jena, Int. J. Quantum Chem. **118**, e25504 (2017).
[29] V. K. Voora and K. D. Jordan, J. Phys. Chem. A **118**, 7201 (2014).
[30] J. P. Rogers, C. S. Anstöter, and J. R. R. Verlet, Nat. Chem. **10**, 341 (2018).
[31] A. Kunin and D. M. Neumark, Phys. Chem. Chem. Phys. **21**, 7239 (2019).
[32] A. Kunin, V. S. McGraw, K. G. Lunny, and D. M. Neumark, J. Chem. Phys. **151**, 154304 (2019).
[33] D. M. Cyr, G. A. Bishea, M. G. Scarton, and M. A. Johnson, J. Chem. Phys. **97**, 5911 (1992).
[34] C. C. Arnold, D. M. Neumark, D. M. Cyr, and M. A. Johnson, J. Phys. Chem. **99**, 1633 (1995).
[35] M. Van Duzor, J. Wei, F. Mbaiwa, and R. Mabbs, J. Chem. Phys. **133**, 144303 (2010).
[36] G. Mensa-Bonsu, D. J. Tozer, and J. R. R. Verlet, Phys. Chem. Chem. Phys. **21**, 13977 (2019).
[37] J. Lyle, T.-C. Jagau, and R. Mabbs, Faraday Discuss. **217**, 533 (2019).
[38] J. E. Mann, M. E. Troyer, and C. C. Jarrold, J. Chem. Phys. **142**, 124305 (2015).
[39] M. A. Duncan, J. Phys. Chem. A **116**, 11477 (2012).
[40] L. A. Posey, M. J. Deluca, and M. A. Johnson, Chem. Phys. Lett. **131**, 170 (1986).
[41] J. M. B. Bakker, J. Phys. E: Sci. Instrum. **6**, 785 (1973).
[42] J. M. B. Bakker, J. Phys. E: Sci. Instrum. **7**, 364 (1974).
[43] A. T. J. B. Eppink and D. H. Parker, Rev. Sci. Instrum. **68**, 3477 (1997).
[44] D. W. Chandler and P. L. Houston, J. Chem. Phys. **87**, 1445 (1987).
[45] M. B. Doyle, C. Abeyasera, and A. G. Suits, "NuAcq 0.9: Native megapixel ion imaging with centroiding to 4 Mpix using inexpensive USB-2 cameras," available at http://faculty.missouri.edu/suitsa/NuAqc.html.
[46] V. Dribinski, A. Ossadtchi, V. A. Mandelshtam, and H. Reisler, Rev. Sci. Instrum. **73**, 2634 (2002).
[47] G. A. Garcia, L. Nahon, and I. Powis, Rev. Sci. Instrum. **75**, 4989 (2004).
[48] F. Weigend and R. Ahlrichs, Phys. Chem. Chem. Phys. **7**, 3297 (2005).
[49] J. Zheng, X. Xu, and D. G. Truhlar, Theor. Chem. Acc. **128**, 295 (2011).
[50] D. Rappoport and F. Furche, J. Chem. Phys. **133**, 134105 (2010).
[51] T. Sommerfeld, K. M. Dreux, and R. Joshi, J. Phys. Chem. A **118**, 7320 (2014).
[52] A. Nakajima, T. Taguwa, K. Hoshino, T. Sugioka, T. Naganuma, F. Oho, K. Watanabe, K. Nakao, Y. Konishi, R. Kishi, and K. Kaya, Chem. Phys. Lett. **214**, 22 (1993).
[53] S. N. Eustis, D. Wang, K. H. Bowen, and G. Naresh Patwari, J. Chem. Phys. **127**, 114312 (2007).
[54] J. P. Rogers, C. S. Anstöter, J. N. Bull, B. F. E. Curchod, and J. R. R. Verlet, J. Phys. Chem. A **123**, 1602 (2019).
[55] J. Korppi-Tommola, H. F. Shurvell, S. J. Daunt, and D. Steele, J. Mol. Spec. **87**, 382 (1981).
[56] T. Sommerfeld, J. B. Melugin, and M. Ehara, J. Phys. Chem. A **122**, 2580 (2018).
[57] D. Steele and D. H. Whiffen, Spectrochim. Acta **16**, 368 (1960).
[58] T. Ridley, D. M. Rogers, and K. P. Lawley, J. Chem. Phys. **141**, 154310 (2014).
[59] N. I. Hammer, K. Diri, K. D. Jordan, C. Desfrançois, and R. N. Compton, J. Chem. Phys. **119**, 3650 (2003).
[60] K. D. Jordan and F. Wang, Annu. Rev. Phys. Chem. **54**, 367 (2003).
[61] R. Mabbs, F. Mbaiwa, J. Wie, M. Van Duzor, S. T. Gibson, S. J. Cavanagh, and B. R. Lewis, Phys. Rev. A **82**, 011401 (2010).
[62] C. S. Anstöter, J. P. Rogers, and J. R. R. Verlet, J. Am. Chem. Soc. **141**, 6132 (2019).